LITHOS 470–471 (2024) 107531

Contents lists available at ScienceDirect

LITHOS

journal homepage: www.elsevier.com/locate/lithos

Iron isotopic compositions of HIMU Ocean island basalts: Implications for the mantle source lithology

Cheng-Cheng Dai [a], Xiao-Jun Wang [a,*], Li-Hui Chen [a], Takeshi Hanyu [b], Xiao-Yu Zhang [c], Gang Zeng [c], Lie-Wen Xie [d]

[a] State Key Laboratory of Continental Dynamics, Department of Geology, Northwest University, Xi'an 710069, China
[b] Research Institute for Marine Geodynamics, Japan Agency for Marine-Earth Science and Technology, Yokosuka 237-0061, Japan
[c] State Key Laboratory for Mineral Deposits Research, School of Earth Sciences and Engineering, Nanjing University, Nanjing 210023, China
[d] State Key Laboratory of Lithospheric Evolution, Institute of Geology and Geophysics, Chinese Academy of Sciences, Beijing 100029, China

ARTICLE INFO

Keywords:
Ocean island basalt
Iron isotopes
HIMU
Source lithology
Carbonated peridotite

ABSTRACT

Basalts from the islands of Mangaia, Tubuai, Rurutu (old stage), and Raivavae (Rairua stage) in the South Pacific, and from St. Helena Island in the South Atlantic, are characterized by extremely radiogenic Pb isotopic compositions (e.g., $^{206}Pb/^{204}Pb > 20.5$). These ocean island basalts (OIBs) define the famous HIMU (high μ, where $\mu = {}^{238}U/^{204}Pb$) component in the mantle 'zoo', which has traditionally been thought to represent ancient recycled oceanic crust with highly fractionated U/Pb and Th/Pb ratios. However, recent high-precision analyses of minor and trace elements in olivine phenocrysts from HIMU OIBs suggest a peridotitic mantle source rather than pyroxenitic/eclogitic remnants of subducted oceanic crust. To better constrain the lithology of the HIMU source is crucial for further understanding the nature of the HIMU component. Here we utilize stable iron (Fe) isotopes, a novel tool for identifying the mantle source lithology of basalts, to further investigate the lithology of the HIMU source by examining classic HIMU OIBs from the Cook-Austral volcanic chain in the South Pacific. The results show that these OIBs have $\delta^{57}Fe$ values varying from 0.09‰ to 0.18‰, which are similar to those of normal mid-ocean ridge basalts (N-MORBs, $\delta^{57}Fe = 0.15 \pm 0.05$‰, 2SD). Quantitative calculations indicate that the fractional-crystallization-corrected $\delta^{57}Fe_{corr}$ values (0.06–0.15‰) of these basalts can well be explained by partial melting of garnet peridotite with $\delta^{57}Fe$ values ranging from 0.05‰ to 0.09‰. Such low $\delta^{57}Fe_{corr}$ values, however, are difficult to be reproduced by partial melting of eclogite with a MORB-like $\delta^{57}Fe$ value ($\delta^{57}Fe = 0.15$‰). Our new Fe isotope data, combined with previously reported heavy whole-rock zinc isotopes ($\delta^{66}Zn = 0.38 \pm 0.03$‰) as well as high Mn/Fe (100Mn/Fe = 1.5–1.7) and Ca/Al (mostly >15) ratios of olivine phenocrysts in the HIMU OIBs, further confirm that the lithology of the HIMU mantle source is carbonated peridotite.

1. Introduction

The significant variation of long-lived radiogenic isotope compositions in oceanic basalts indicates a highly heterogeneous mantle, which encompasses several mantle components with distinct isotopic characteristics: DMM (depleted MORB mantle), FOZO (focus zone; Hart et al., 1992), EM1 (enriched mantle 1), EM2 (enriched mantle 2), and HIMU (high μ, where $\mu = {}^{238}U/^{204}Pb$) (e.g., Hanyu and Chen, 2021; Hofmann, 1997; Stracke, 2012; White, 2015; Zindler and Hart, 1986). The classic HIMU component is defined by ocean island basalts (OIBs) from Cook-Austral islands (Mangaia, Tubuai, Old Rurutu, Old Raivavae) in the South Pacific and the Saint Helena (St. Helena) Island in the South Atlantic. This mantle component stands out for its extremely high $^{206}Pb/^{204}Pb$ (> 20.5) and low $^{87}Sr/^{86}Sr$ (~ 0.7028) ratios. Meanwhile, its $^{208}Pb/^{204}Pb$ ratios are plotted beneath the northern hemisphere reference line (NHRL; Hart, 1984) on the $^{208}Pb/^{204}Pb$ versus $^{206}Pb/^{204}Pb$ diagram, and the Sr-Nd-Hf isotopic compositions are projected below the DMM-EM mantle array (e.g., Hanyu et al., 2014; Homrighausen et al., 2018; Kawabata et al., 2011; Stracke et al., 2005; White, 2015; Zindler and Hart, 1986).

The origin of the HIMU component has traditionally been attributed to the recycling of ancient altered oceanic crust: hydrothermal alteration and dehydration during oceanic slab subduction produced the high U/Pb and Th/Pb ratios of the subducted oceanic crust and therefore can

* Corresponding author.
E-mail address: wangxj@nwu.edu.cn (X.-J. Wang).

https://doi.org/10.1016/j.lithos.2024.107531
Received 8 November 2023; Received in revised form 4 February 2024; Accepted 4 February 2024
Available online 7 February 2024

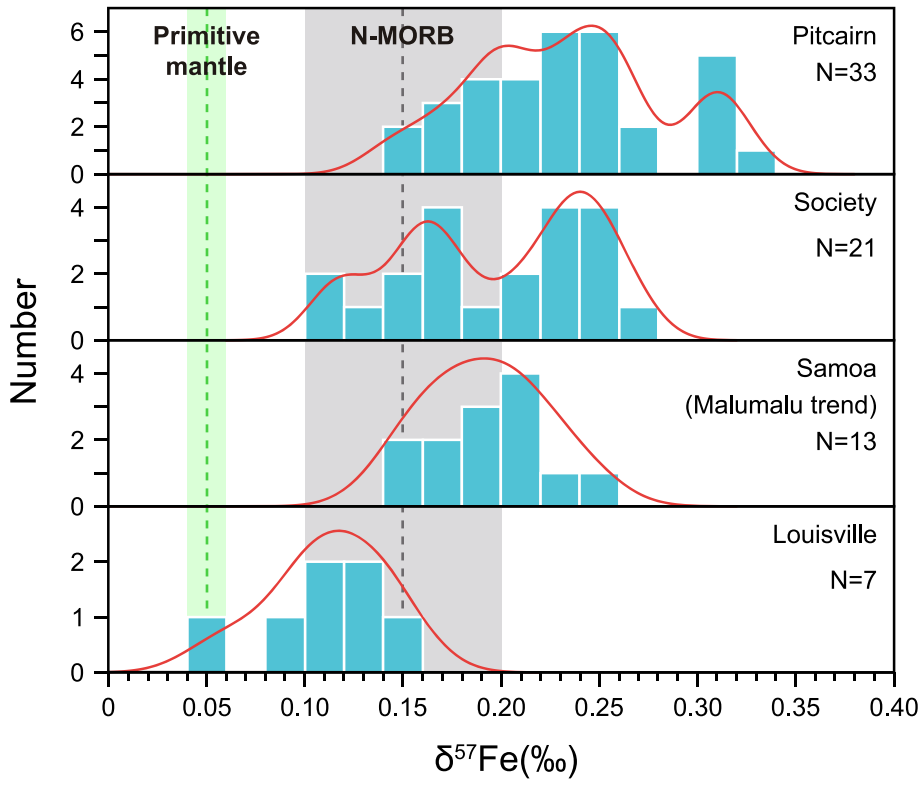

Fig. 1. Iron isotopic compositions of representative endmember OIBs. The vertical green and gray bands represent the Fe isotopic ranges for primitive mantle ($\delta^{57}Fe = 0.05 \pm 0.01$ ‰, 2SE; Sossi et al., 2016) and N-MORBs ($\delta^{57}Fe = 0.15 \pm 0.05$ ‰, 2SD;Gleeson et al., 2020; Teng et al., 2013), respectively. The Pitcairn Island/seamounts are type localities for the EM1 component, while the Samoa and Society islands/seamounts are type localities for the EM2 component. The Louisville seamount chain sampled the FOZO component. Data sources for Fe isotopes: Louisville (Shi et al., 2022), Society (Teng et al., 2013); Samoa (Soderman et al., 2021; Wang et al., 2021), Pitcairn (Nebel et al., 2019; Shi et al., 2022). (For interpretation of the references to colour in this figure legend, the reader is referred to the web version of this article.)

explain the extremely radiogenic Pb isotopic compositions of the HIMU component after long-term isolation in the lower mantle (e.g., Cabral et al., 2013; Chauvel et al., 1992; Hofmann and White, 1982; Kimura et al., 2016; Stracke, 2012; Zindler and Hart, 1986). However, some recent studies tend to support models in which subducted oceanic crust contributed to the formation of the HIMU component through an indirect way (e.g., Hanyu et al., 2011a; Herzberg et al., 2014; Wang et al., 2024; Weiss et al., 2016; Zhang et al., 2022). For instance, recycled oceanic crust has a very high Re/Os ratio, which should lead to extremely high $^{187}Os/^{188}Os$ (> 1) after long-term (billions of years) isolated evolution (e.g., Hanyu et al., 2011a). Thus, Hanyu et al. (2011a) suggested that the moderately high $^{187}Os/^{188}Os$ (0.14–0.15) ratios of HIMU lavas cannot be directly attributed to the long-term evolution of recycled oceanic crust, but require the mixing of melts derived from subducted oceanic crust and surrounding peridotitic mantle. Additionally, the olivine phenocrysts in HIMU lavas have low Ni contents and high Mn/Fe ratios, indicating a peridotite-dominated source rather than pyroxenitic remnants of recycled oceanic crust (Herzberg et al., 2014). Herzberg et al. (2014) thus proposed that the HIMU source is predominantly composed of refertilized peridotite, resulting from the injection of silicic melts released by recycled oceanic crust into the nearby mantle peridotite. Furthermore, based on the trace-element compositions of olivine phenocrysts in HIMU lavas and the similar incompatible trace-element patterns between HIMU OIBs and carbonatitic melt inclusions in diamonds, Weiss et al. (2016) suggested that the HIMU component originates from carbonatite-metasomatized subcontinental lithospheric mantle (SCLM) linked to the subduction of ancient oceanic crust. The newly-reported heavy zinc isotopic compositions ($\delta^{66}Zn = 0.38 \pm 0.03$‰) of the classic HIMU OIBs were also attributed to a carbonated source (Zhang et al., 2022). The formation of this source involves two main processes: 1) the partial melting of ancient subducted oceanic crust and overlying carbonates in the deep mantle, resulting in carbonate-bearing melts; and 2) the carbonate-bearing melts metasomatize the surrounding peridotite, leading to the formation of a carbonated source (Zhang et al., 2022). Overall, the inferred lithology of the HIMU source in these recent models should be refertilized/metasomatized peridotite. While in terms of the classic oceanic-crust-recycling model, the source lithology of the HIMU OIBs is expected to be eclogite or pyroxenite transformed from subducted oceanic crust. Therefore, further identification of the source lithology is necessary to evaluate the different models for the origin of the HIMU component.

Iron stable isotopes are emerging as an effective tool for identifying the source lithology of OIBs (e.g., Gleeson et al., 2020; Konter et al., 2016; Nebel et al., 2019; Shi et al., 2022; Soderman et al., 2021; Wang et al., 2021; Williams and Bizimis, 2014). The Fe^{3+}-free minerals (e.g., olivine) prefer the lighter Fe isotopes (e.g., ^{54}Fe) compared to minerals containing Fe^{3+} (e.g., Polyakov and Mineev, 2000; Sossi and O'Neill, 2017), and melts derived from an olivine-dominated mantle lithology (e.g., peridotite) will show lower $\delta^{57}Fe$ ($\delta^{57}Fe = [(^{57}Fe/^{54}Fe)_{sample}/(^{57}Fe/^{54}Fe)_{IRMM\text{-}014} - 1]*1000$) than those derived from a pyroxene-dominated lithology (e.g., pyroxenite) (e.g., Gleeson et al., 2020; Konter et al., 2016; Soderman et al., 2021, 2023; Williams and Bizimis, 2014). The feasibility of using Fe isotopes to identify the source lithology of OIBs is also supported by the Fe isotope dataset for OIBs from the type localities for the EM and FOZO mantle components (Fig. 1). The FOZO-type OIBs from the Louisville Seamount Chain, previously thought to be fed by a normal peridotite source (e.g., Shi et al., 2022; Zhong et al., 2017), exhibit Fe isotope compositions similar to N-MORBs ($\delta^{57}Fe =$ 0.06–0.15‰; Shi et al., 2022; Fig. 1). In contrast, EM-type OIBs display obviously heavier Fe isotope compositions relative to N-MORBs,

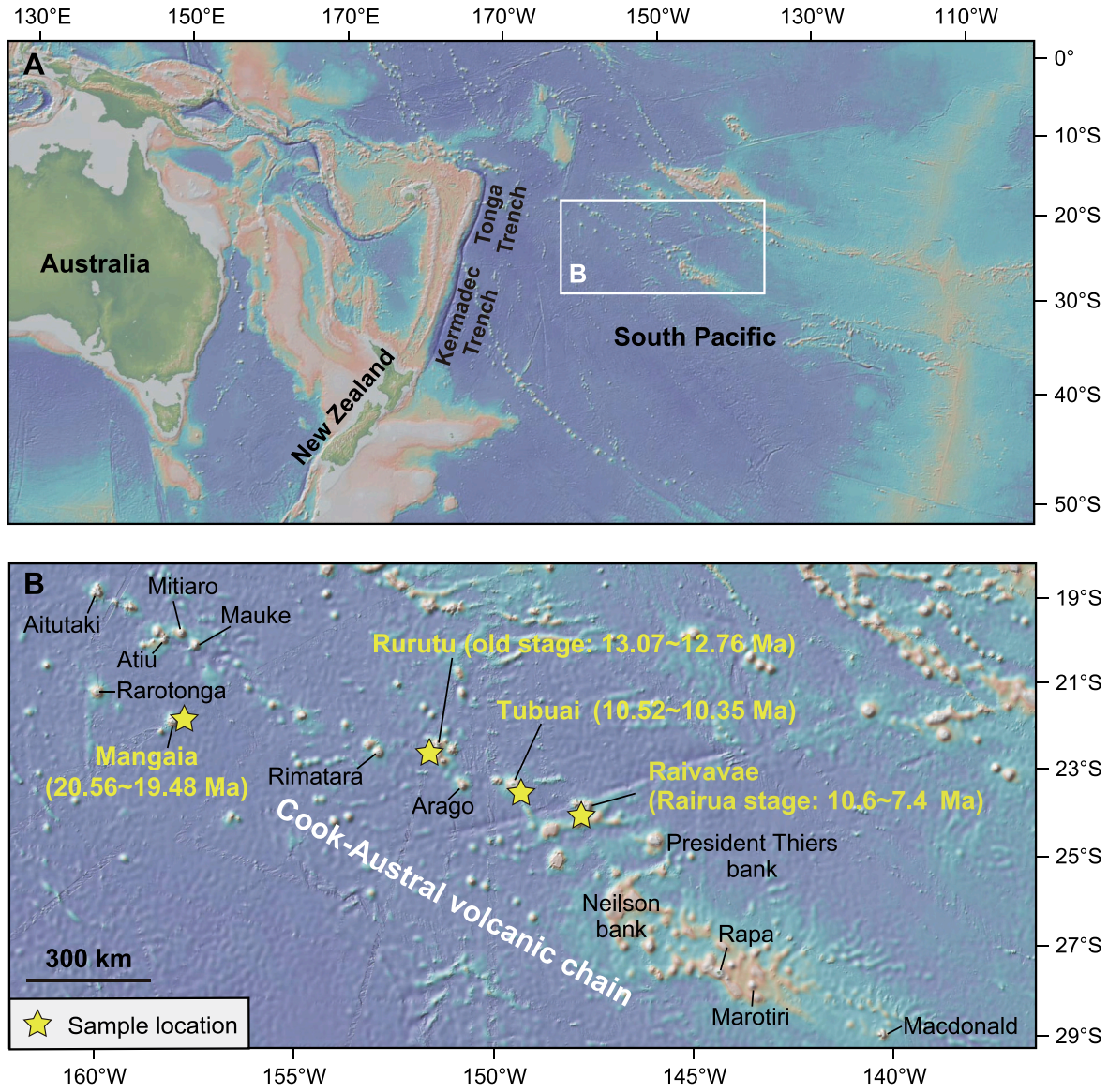

Fig. 2. (A) Topographic map showing the location of the Cook-Austral volcanic chain. (B) Topographic map of the Cook-Austral volcanic chain. The ages for Mangaia, Rurutu (old stage), and Tubuai are from Rose and Koppers (2019). The ages for Raivavae (Rairua stage) are from Maury et al. (2013). The topographic maps were generated from the GeoMapApp (http://www.geomapapp.org) (Ryan et al., 2009). (For interpretation of the references to colour in this figure legend, the reader is referred to the web version of this article.)

suggesting the contribution of eclogite/garnet pyroxenite in their mantle sources (Fig. 1) (Nebel et al., 2019; Shi et al., 2022; Soderman et al., 2021; Wang et al., 2021). Therefore, Fe isotopic compositions of HIMU OIBs are expected to provide further constraints on the lithological characteristics of their source regions.

In this study, we present new high-precision Fe isotopic data of classic HIMU OIBs from the Cook-Austral volcanic chain in the South Pacific. The results show that all the investigated HIMU lavas have relatively homogeneous, normal MORB-like Fe isotopic compositions ($\delta^{57}Fe$ = 0.09–0.18‰), indicating a peridotitic mantle source. This observation, combined with previously reported elemental and isotopic data from the same suite of HIMU OIBs, will be utilized to further evaluate the origin of the HIMU mantle component.

2. Geological background and sample description

The investigated OIB samples in this study are from four islands (Mangaia, Rurutu, Tubuai, and Raivavae; Fig. 2) that are part of the Cook-Austral volcanic chain in the South Pacific. This ~2000 km long volcanic chain consists of thirteen islands and numerous seamounts (Fig. 2), believed to have been produced by deep-rooted mantle plumes (e.g., French and Romanowicz, 2015; Rose and Koppers, 2019). The Mangaia, Rurutu, and Tubuai islands have newly reported $^{40}Ar/^{39}Ar$ ages of 20.56–19.48 Ma, 13.07–12.76 Ma (older eruption), and 10.52–10.35 Ma, respectively (Rose and Koppers, 2019). The Raivavae Island was built by two successive volcanic events: the Rairua-stage (10.6–7.4 Ma) and the Anatonu-stage (6.4–5.4 Ma) (Maury et al., 2013).

Comprehensive petrological and geochemical analyses, including major and trace elements, radiogenic Sr, Nd, Pb, Hf, He, and Os isotopes, as well as stable Zn and Ca isotopes, of these OIBs have been well documented and reported elsewhere (Hanyu et al., 2011a; Hanyu and Kaneoka, 1997; Miyazaki et al., 2018; Wang et al., 2024; Zhang et al., 2022). The photomicrographs of thin sections for the studied HIMU OIBs revealed no obvious post-eruptive alteration, except for partial idding-sitization of olivine rims in rare cases (Hanyu et al., 2011a). In addition, most samples display low Ba/Rb (< 20, **Table S1**) and K/Rb ratios (< 500, **Table S1**) as those of fresh OIBs (e.g., Ba/Rb < 30, K/Rb < 1000; Pietruszka et al., 2013), suggesting limited effects of potential alteration

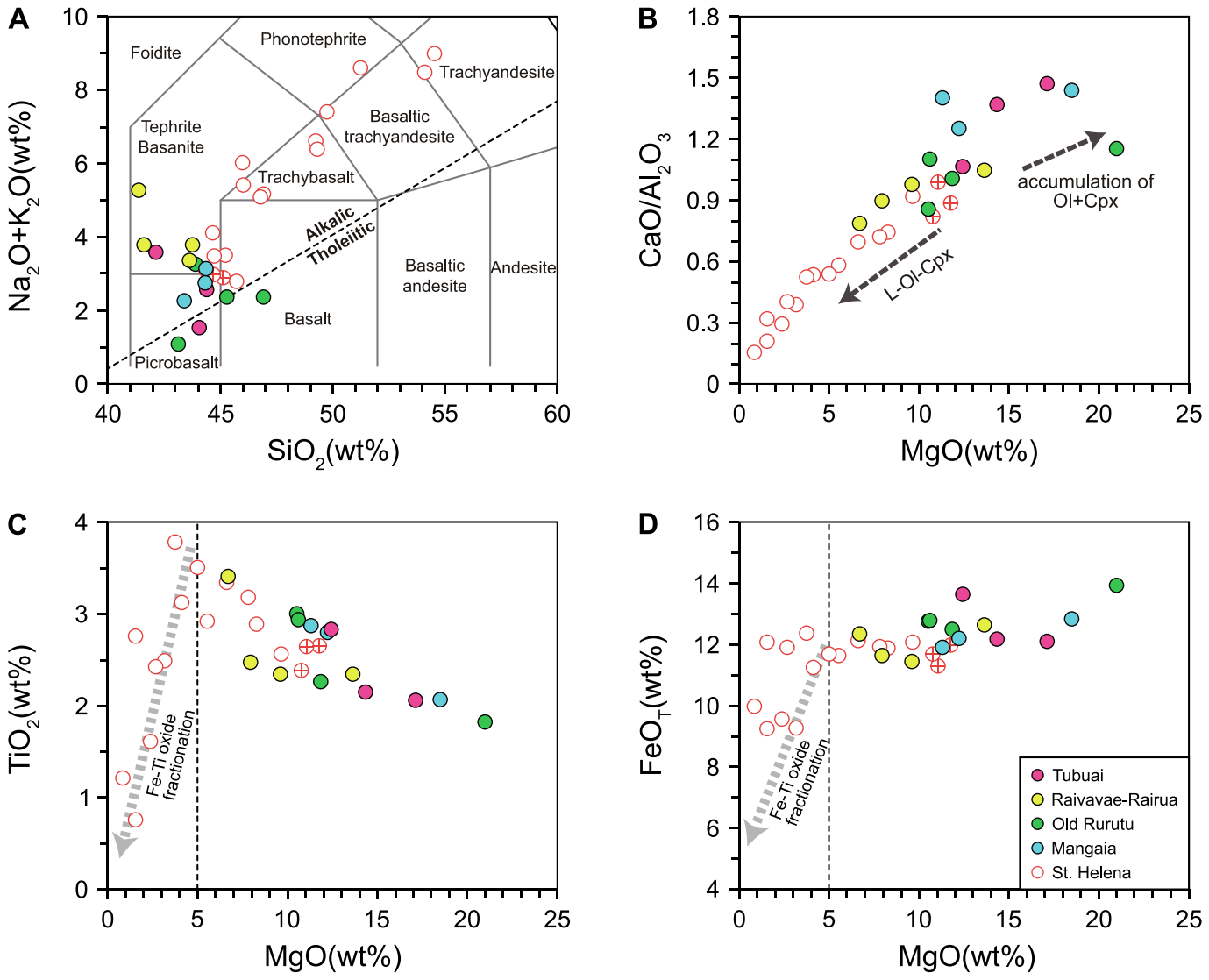

Fig. 3. Major element variations for Cook-Austral HIMU OIB samples. The data are from Hanyu et al. (2011a) and Miyazaki et al. (2018). Previously studied St. Helena samples with published Fe isotope data were also plotted for comparison, and the data are from Kawabata et al. (2011). (A) Total alkalis ($Na_2O + K_2O$) versus SiO_2 diagram (after Le Bas et al., 1986). The dashed line represents the division of alkalic-tholeiitic series (MacDonald and Katsura, 1964). (B-D) CaO/Al_2O_3, TiO_2, and FeO_T (total iron) versus MgO contents. Three St. Helena samples with high MgO contents (> 10 wt%; marked by red circles with crosses) have chemical compositions close to those of St. Helena primary melts (Kawabata et al., 2011). (For interpretation of the references to colour in this figure legend, the reader is referred to the web version of this article.)

on the chemical compositions of these samples. Most samples are classified as alkaline basalts and are plotted within the fields of tephrite/basanite, picrobasalt, and basalt on the total-alkali versus silica diagram (Fig. 3A). The Cook-Austral lavas show low SiO_2 (41.34–46.90 wt%) contents and high CaO/Al_2O_3 ratios (0.79–1.47) (Figs. 3A-3B). These lavas display extremely high $^{206}Pb/^{204}Pb$ (20.6–21.4), intermediate $^{143}Nd/^{144}Nd$ (0.51283–0.51292) and $^{176}Hf/^{177}Hf$ (0.28290–0.28298), as well as low $^{87}Sr/^{86}Sr$ (0.70277–0.70284) ratios (Hanyu et al., 2011a; Kawabata et al., 2011; **Fig. S1**). These OIBs also show relatively uniform and slightly lower $^{3}He/^{4}He$ ratios of 6.02–7.42 R_A (Hanyu et al., 2011b; Hanyu and Kaneoka, 1997) compared to global MORBs (8.75 ± 2.14 R_A; Graham, 2002). In addition, these lavas are characterized by moderately radiogenic $^{187}Os/^{188}Os$ (0.14–0.15; Hanyu et al., 2011a) and heavy Zn isotopic compositions ($\delta^{66}Zn = 0.37 \pm 0.03‰$; Zhang et al., 2022).

3. Analytical methods

3.1. Iron isotope analysis

Iron isotopic analyses were performed at the Institute of Geology and Geophysics, Chinese Academy of Science, using an analytical procedure modified from Dauphas et al. (2004). The detailed procedures can be found in Wang et al. (2021) and Shi et al. (2022). About 10–30 mg of sample powders and USGS (the United States Geological Survey) reference materials were completely digested by concentrated double-distilled acids in the Savillex screw-top beakers, according to the following sequence: (i) digestion in HF-HNO_3, (ii) digestion in HCl-HNO_3 (3:1, vol/vol), and (iii) digestion in HCl. Subsequently, the clear solutions were dried and dissolved in 6 mol/L HCl with Fe concentration of 100 μg/mL for ion exchange purification. Iron purification was achieved by anion exchange process in Savillex microcolumns loaded with 2 mL of pre-cleaned Bio-Rad AG1-X8 (38–74 μm) anion resin. 8 mL of 6 mol/L HCl (in a sequence 0.5, 0.5, 1, 2, and 4 mL) and 0.5 mL of 0.4 mol/

Table 1
Iron isotopic compositions of ocean island basalts from the Cook-Austral volcanic chain, South Pacific.

Sample name	Location	$\delta^{56}Fe$[a]	2SD[b]	$\delta^{57}Fe$	2SD	N	$Fe^{3+}/\Sigma Fe$	$\delta^{57}Fe_{corr}$[c]
MGA301	Mangaia	0.07	0.01	0.10	0.03	3	0.28	0.08
MGA303–1	Mangaia	0.08	0.04	0.11	0.06	4	0.17	0.11
MGA303–1 re[d]	Mangaia	0.09	0.02	0.13	0.04	4		0.13
MGA307	Mangaia	0.11	0.01	0.17	0.06	3	0.24	0.15
RRT302–1	Old Rurutu	0.08	0.01	0.12	0.03	3	0.28	0.09
RRT304–2	Old Rurutu	0.06	0.05	0.10	0.06	4	0.20	0.07
RRT306	Old Rurutu	0.06	0.01	0.09	0.04	4	0.23	0.06
RRT303	Old Rurutu	0.10	0.02	0.13	0.03	3		0.13
TBA301–1	Tubuai	0.10	0.03	0.16	0.04	4	0.32	0.13
TBA303–3	Tubuai	0.06	0.03	0.10	0.04	4	0.29	0.09
TBA304–5	Tubuai	0.06	0.02	0.09	0.02	4	0.25	0.09
RAV-05	Raivavae-Rairua	0.08	0.02	0.14	0.04	3	0.39	0.10
RAV-11	Raivavae-Rairua	0.11	0.05	0.18	0.06	4	0.34	0.12
RAV-11 re	Raivavae-Rairua	0.12	0.03	0.17	0.06	4		0.11
RAV-20	Raivavae-Rairua	0.11	0.03	0.16	0.06	4	0.33	0.13
RAV-34	Raivavae-Rairua	0.09	0.05	0.15	0.06	4	0.22	0.13

[a] $\delta^{X}Fe = ([^{X}Fe/^{54}Fe]_{sample}/[^{X}Fe/^{54}Fe]_{IRMM\text{-}014} - 1) \times 1000$, where X = 56 or 57 and IRMM-014 is an international Fe isotope standard.
[b] 2SD represents two standard deviations of N ($N \geq 3$) times repetitive measurements of the same sample.
[c] $\delta^{57}Fe_{corr}$: Fe isotope data have been corrected for fractional crystallization (see Section 5.1 for detail).
[d] "re" denotes repeating sample digestion, column chemistry and instrumental analysis.

L HCl were used to elute matrix elements, and then iron was eluted by 11.5 mL of 0.4 mol/L HCl. Purified solutions were evaporated to dryness and diluted to 3 μg/mL Fe using the same batch of 2% HNO_3 for measurement. After the chemical purification procedures, the Fe recovery was ≥99.8% for all analyzed reference materials and unknown samples.

Iron isotopic compositions were determined on a Thermo Scientific Neptune MC-ICP-MS in high-resolution mode (M/ΔM > 9000 as defined by the peak edge width from 5 to 95% full peak height), using sample-standard bracketing method. ^{53}Cr, ^{54}Fe, ^{56}Fe, ^{57}Fe, ^{58}Fe and ^{60}Ni were collected by a multi-collector Faraday cup configuration of L3, L1, C, H1, H2 and H4, respectively. The approximate signal intensity for ^{56}Fe was 3–4 V/ppm, and the signal contribution from blank was typically <2 mV. Iron isotope data are reported in δ-notation as per mil (‰) deviation from IRMM-014: $\delta^{X}Fe = [(^{X}Fe/^{54}Fe)_{sample}/(^{X}Fe/^{54}Fe)_{IRMM\text{-}014} - 1] \times 1000$, where X is 56 or 57. The reported Fe isotope ratios for each sample are average values of multiple duplicate analyses (at least three times). The external reproducibility for $\delta^{57}Fe$ is better than 0.07‰ (2SD) based on hundreds of replicated analyses of international standard (JMC Fe) and different igneous reference materials. In this study, repeated measurements of in-house Fe standard IGG Fe (GSB Fe, an ultrapure single element standard solution) and JMC Fe at different dates give averaged $\delta^{57}Fe$ values of 1.08 ± 0.05‰ (2SD, $n = 72$) and 0.56 ± 0.02‰ (2SD, $n = 18$), respectively. These values exhibit excellent agreement with previously reported results (**Table S2**).

3.2. $Fe^{3+}/\Sigma Fe$ analysis

The $Fe^{3+}/\Sigma Fe$ ratios were determined by back titration method at the State Key Laboratory for Mineral Deposits Research, Nanjing University, following the method of Shi et al. (2022). The FeO contents were determined by redox titration using ammonium metavanadate. Sample powders were digested using 10 mL concentrated HF and 5 mL concentrated H_2SO_4. To ensure complete dissolution, the samples were first agitated in an ultrasonic bath for 20 min and then heated on a 100 °C hotplate overnight. The solutions were then buffered by saturated boric acid. After this step, 10 mL H_3PO_4-H_2SO_4 mixed acids were added into the solutions to improve the accuracy of end-point detection. Finally, the solutions were titrated with 0.05 mol/L $(NH_4)_2Fe(SO_4)_2$ titrant until the volume of titrant was recorded at the point of maximum slope of the titration curve. The volume of the spent titrant can be used to calculate the FeO concentration and $Fe^{3+}/\Sigma Fe$ ratio. The determined FeO concentration (10.01 ± 0.03 wt%, 2SD, $N = 4$) and $Fe^{3+}/\Sigma Fe$ ratio (0.221 ± 0.003, 2SD, N = 4) of the JB-2 reference material agree well with the recommended values (FeO = 9.98 wt%, $Fe^{3+}/\Sigma Fe = 0.23$; Imai et al., 1995).

4. Results

The Fe isotope data and $Fe^{3+}/\Sigma Fe$ values of the studied Cook-Austral HIMU OIB samples are presented in Table 1 and illustrated in Fig. 4. The $\delta^{57}Fe$ values of the Cook-Austral OIB samples range from 0.09 ± 0.02‰ to 0.18 ± 0.06‰ (2SD) and are similar to those of the relatively primitive St. Helena HIMU OIBs (e.g., when MgO > 10 wt%, $\delta^{57}Fe$ values vary from 0.04 ± 0.04‰ to 0.19 ± 0.03‰; Zhao et al., 2022). In general, the primitive HIMU OIBs from both the Cook-Austral volcanic chain and the St. Helena Island display normal MORB-like ($\delta^{57}Fe = 0.15 \pm 0.05$‰; Gleeson et al., 2020; Teng et al., 2013) Fe isotopic compositions (Fig. 4). The $Fe^{3+}/\Sigma Fe$ ratios of the Cook-Austral OIB samples vary from 0.17 to 0.39 (with a mean value of 0.27; Table 1), which are comparable to those of the high-MgO (e.g., > 10 wt%) St. Helena HIMU OIBs (Fig. 4C) and fall within the $Fe^{3+}/\Sigma Fe$ range (0.09–0.40) observed in the least degassed OIB glasses globally (e.g., Brounce et al., 2022). In addition, there is a negative correlation between $Fe^{3+}/\Sigma Fe$ ratios and MgO contents of all the HIMU OIBs, implying that the primary HIMU lavas may have a $Fe^{3+}/\Sigma Fe$ ratio of ~0.2 (Fig. 4C).

5. Discussion

5.1. Magma differentiation

The studied Cook-Austral OIB samples have a wide range of MgO contents (MgO = 6.68–21.00 wt%), indicating potential effects of fractional crystallization and mineral accumulation. Previous study has found that the three samples with very high MgO contents (> 17 wt%) contain some accumulated minerals, including olivine and minor clinopyroxene (Hanyu et al., 2011a). The remaining samples show a positive correlation between MgO and CaO/Al_2O_3 ratios (Fig. 3B), suggesting that these samples have undergone fractional crystallization of olivine and clinopyroxene to varying degrees. This is consistent with the occurrence of olivine and clinopyroxene phenocrysts in these samples (Hanyu et al., 2011a; Miyazaki et al., 2018). The relatively high MgO contents (> 6 wt%) and the lack of a positive correlation between MgO and TiO_2 (or FeO_T) (Figs. 3C-D) indicate that these samples have not undergone the fractionation of Fe-Ti oxides.

Previous studies have shown that the fractional crystallization process can significantly affect the iron isotopic compositions of basaltic lavas: the segregation of isotopically light olivine and clinopyroxene (relative to melt) can lead to an increase in $\delta^{57}Fe$ values of residual

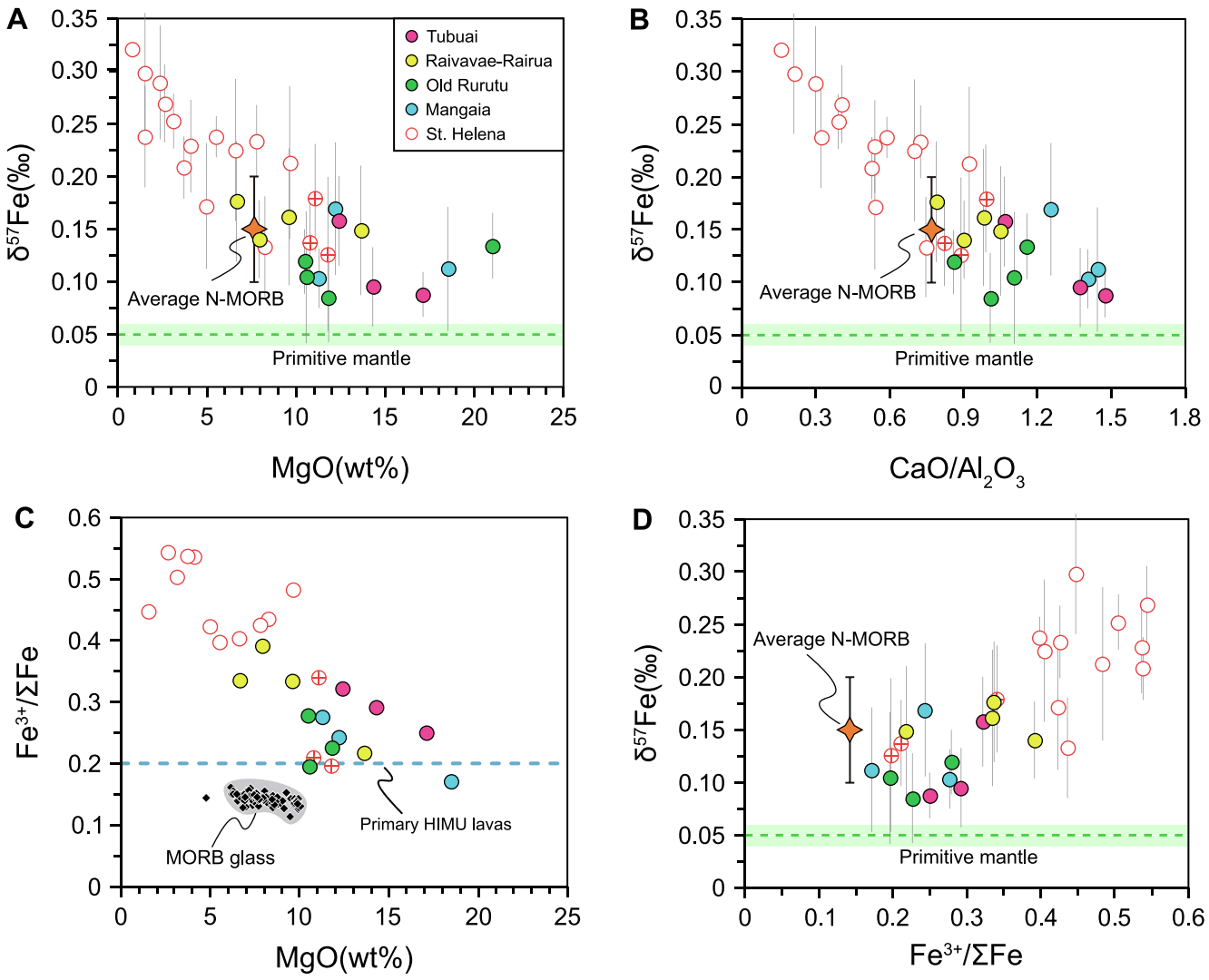

Fig. 4. (A) $\delta^{57}Fe$ versus MgO, (B) $\delta^{57}Fe$ versus CaO/Al_2O_3, (C) $Fe^{3+}/\Sigma Fe$ versus MgO, and (D) $\delta^{57}Fe$ versus $Fe^{3+}/\Sigma Fe$ for Cook-Austral HIMU OIB samples. Literature data for St. Helena samples are from Kawabata et al. (2011) and Zhao et al. (2022). The $\delta^{57}Fe$ range for average N-MORB is calculated from the reported $\delta^{57}Fe$ values in Gleeson et al. (2020) and Teng et al. (2013). The $\delta^{57}Fe$ value (0.05 ± 0.01‰, 2SE) of the primitive mantle is from Sossi et al. (2016). The $Fe^{3+}/\Sigma Fe$ values of MORB glasses are from Zhang et al. (2018). Three St. Helena samples with high MgO contents (> 10 wt%; marked by red circles with crosses) have chemical and Fe isotopic compositions close to those of St. Helena primary melts (Kawabata et al., 2011; Zhao et al., 2022). Thus, their average chemical and isotopic compositions are regarded as the primitive compositions of St. Helena OIBs in the following figures. According to the negative correlation between $Fe^{3+}/\Sigma Fe$ ratios and MgO contents of the HIMU lavas, we assume that $Fe^{3+}/\Sigma Fe$ of ~0.2 is close to that of primary HIMU magmas. Error bars represent 2SD (two times standard deviation) uncertainties. (For interpretation of the references to colour in this figure legend, the reader is referred to the web version of this article.)

melts, while the fractional crystallization of different types of Fe-Ti oxides can drive the residual melts towards higher or lower $\delta^{57}Fe$ values (e.g., Chen et al., 2019; Chen et al., 2021; McCoy-West et al., 2018; Schuessler et al., 2009; Sossi et al., 2012; Teng et al., 2008; Williams et al., 2018; Zhao et al., 2022). In this study, all of the Cook-Austral OIB samples are less evolved ones (MgO > 5 wt%, Figs. 3C-D) that have not undergone the fractionation of Fe-Ti oxides, thus precluding the influence of Fe-Ti oxide fractionation on their Fe isotopic compositions.

In order to obtain the Fe isotopic compositions of primary magmas for the Cook-Austral samples, we follow the approach of Sossi et al. (2016) to restore the chemical compositions of each sample to its primary melt compositions that are in Fe-Mg equilibrium with Fo_{90} mantle. It is worth noting that the uncertainty introduced by choosing different equilibrated olivine compositions (e.g., Fo_{90} or Fo_{85}) is less than the uncertainty in applying the correction method (e.g., Sossi et al., 2016). We incrementally added olivines that are in Fe-Mg equilibrium with the melt compositions into the melts. At each incremental step, we used a Fe-Mg partition coefficient ($K_{D_{Ol-Melt}}^{Fe-Mg}$) of 0.32 to recalculate the compositions of both the olivines and the melts. The $\delta^{57}Fe$ values of olivines and melts were calculated based on an olivine-melt fractionation factor ($\Delta^{57}Fe_{Ol-melt}$) of $-0.3 \times 10^6/T^2$ (Sossi et al., 2016). This fractionation factor has been demonstrated to be the most reasonable one to reproduce the Fe isotopic evolution paths in cogenetic mafic magmas (e.g., Chen et al., 2019; Sossi et al., 2016; Teng et al., 2008; Zhao et al., 2022). Additionally, given the small difference between $\Delta^{57}Fe_{Ol-melt}$ ($-0.3 \times 10^6/T^2$) and $\Delta^{57}Fe_{Cpx-melt}$ ($-0.25 \times 10^6/T^2$; Sossi et al., 2012), we only corrected for olivine crystallization as in many previous studies (e.g., Soderman et al., 2021; Sossi et al., 2016; Wang et al., 2021). In order to minimize the uncertainty introduced by correcting the Fe isotopic compositions of different samples, this method has also been applied to published OIB and MORB data.

The fractional-crystallization-corrected $\delta^{57}Fe_{corr}$ values of our Cook-Austral samples range from 0.06‰ to 0.15‰ (Table 1), which are still comparable to the average $\delta^{57}Fe_{corr}$ value of N-MORBs (0.10 ± 0.05‰, 2SD; Gleeson et al., 2020; Teng et al., 2013). The three high-MgO (> 17 wt%) Cook-Austral samples containing accumulated olivines show no

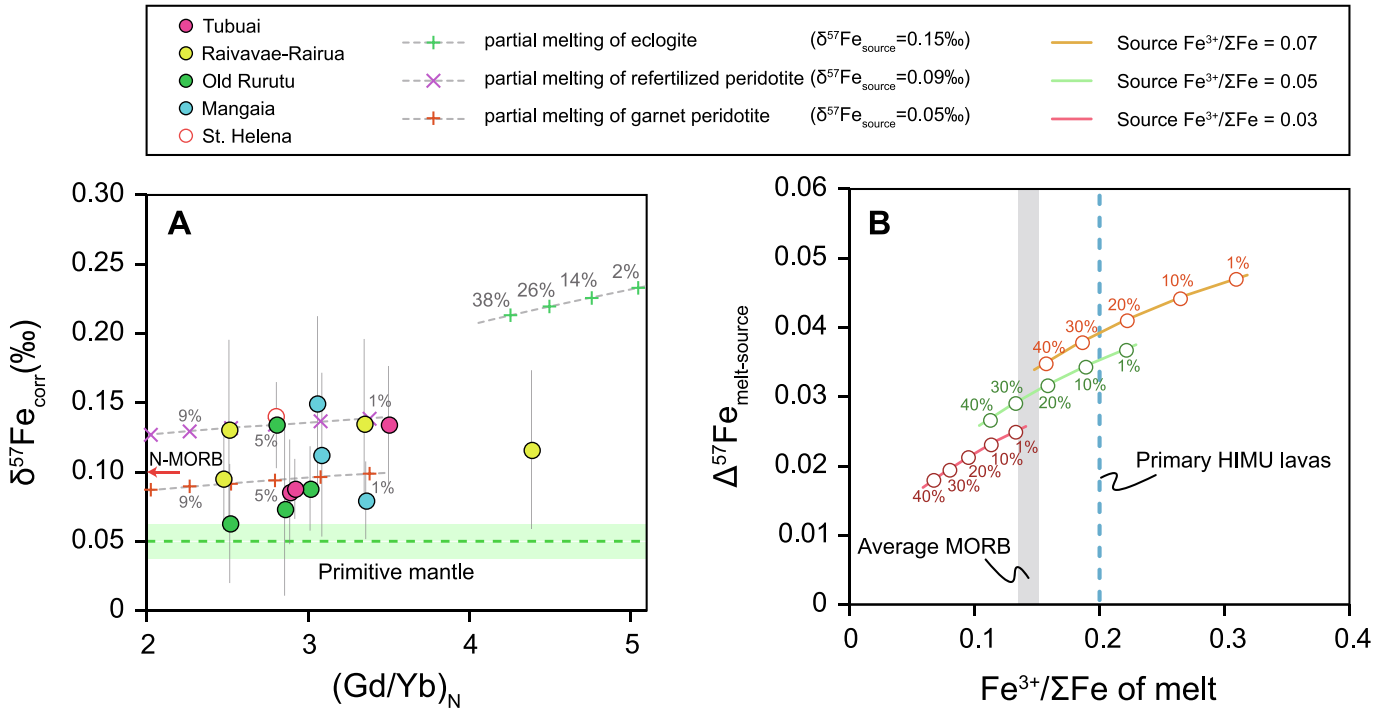

Fig. 5. (A) $\delta^{57}Fe_{corr}$ versus $(Gd/Yb)_N$ for Cook-Austral HIMU OIB samples. The subscript N denotes normalized to primitive mantle value (McDonough and Sun, 1995). The Fe isotopic compositions and trace element data of St. Helena primary magmas are from Zhao et al. (2022) and Kawabata et al. (2011), respectively. The Gd and Yb concentrations of Cook-Austral HIMU OIB samples are from Hanyu et al. (2011a), Miyazaki et al. (2018), and Zhang et al. (2022). The Fe isotopic compositions of average N-MORB and the primitive mantle are from Sossi et al. (2016). Quantitative calculations for the partial melting of garnet peridotite and eclogite are given in Table S3 and Table S4, respectively. (B) Calculated Fe isotope fractionation during partial melting ($\Delta^{57}Fe_{melt-source}$) under different source redox conditions. The related equations and parameters (except for the $Fe^{3+}/\Sigma Fe$ value of mantle source) are the same as in Dauphas et al. (2014). Note the very small difference in the extent of Fe isotope fractionation during partial melting under distinct source redox conditions. The $Fe^{3+}/\Sigma Fe$ range of average MORB is from Zhang et al. (2018). Error bars represent 2SD uncertainties.

statistical $\delta^{57}Fe$ difference compared to the other samples (Fig. 4A). Therefore, following Soderman et al. (2021), we will include the uncorrected $\delta^{57}Fe$ values of these high-MgO samples in the subsequent figures. In addition, the $\delta^{57}Fe$ value of the St. Helena primary magma was previously estimated at 0.13 ± 0.06‰ (Zhao et al., 2022), and this value will be used in the following discussions together with our calculated $\delta^{57}Fe_{corr}$ values for the Cook-Austral HIMU OIBs.

5.2. Partial melting and redox conditions

The detectable Fe isotopic difference between primary, mantle-derived magmas and mantle peridotite has generally been attributed to Fe isotope fractionation during the partial melting of the mantle (e.g., Chen et al., 2019; Craddock et al., 2013; Dauphas et al., 2009; Soderman et al., 2021; Teng et al., 2013; Weyer and Ionov, 2007; Williams et al., 2005). This coincides with the theoretical predictions that oxidized Fe^{3+} tends to form shorter and more robust Fe-O bonds, and therefore prefers heavy Fe isotopes (e.g., Dauphas et al., 2014; Polyakov and Mineev, 2000; Sossi and O'Neill, 2017). During partial melting of the mantle, the incompatible Fe^{3+} preferentially enters the melt, causing the heavy Fe isotopes to concentrate in the melt (e.g., Dauphas et al., 2009, 2014; Sossi and O'Neill, 2017; Williams and Bizimis, 2014).

In order to evaluate the effects of mantle partial melting on the Fe isotopic compositions of basalts, we quantitively modelled the variations of $\delta^{57}Fe$ and Gd/Yb_N (where subscript N denotes primitive-mantle-normalized) values during partial melting of garnet peridotite and eclogite (see **Tables S3–S4** for details). The calculation methods are modified from Wang et al. (2021) and are similar to those used in previous studies (e.g., Gleeson et al., 2020; Sossi and O'Neill, 2017; Williams and Bizimis, 2014). We used non-modal batch melting equations to calculate the concentrations of iron in the melt and residue. We calculated the mineral-melt Fe isotope fractionation factors ($\Delta^{57}Fe_{mineral-melt}$) based on the Fe-O force constants of mantle minerals and basaltic melts (Dauphas et al., 2014; Sossi and O'Neill, 2017). A mass balance approach was utilized to calculate the $\delta^{57}Fe$ values of melts and residues at each melting increment (see **Tables S3–S4** for details). The Fe isotopic fractionation during mantle partial melting estimated by this method (**Tables S3 and S4**) shows no significant difference compared to that calculated by thermodynamic models (e.g., Soderman et al., 2021, 2022). The initial $\delta^{57}Fe$ value of the garnet peridotite was assumed to be equal to the primitive mantle value (0.05‰; Sossi et al., 2016). Results show that partial melting of such a garnet peridotite source can produce melts with $\delta^{57}Fe$ values of 0.08–0.10‰ (Fig. 5A), which is close to the average $\delta^{57}Fe$ value of primary N-MORBs ($\delta^{57}Fe_{corr}$ = 0.10 ± 0.05‰, 2SD; e.g., Gleeson et al., 2020; Teng et al., 2013). For the melting of eclogite that transformed from subducted oceanic crust, we assumed the initial source $\delta^{57}Fe$ value to be equal to the average value of N-MORBs (0.15‰; Teng et al., 2013). The calculated $\delta^{57}Fe$ values of melts derived from such an eclogite source range from 0.19‰ to 0.23‰ (Fig. 5A), which are apparently higher than those of peridotite-derived basalts (e.g., N-MORB; $\delta^{57}Fe_{corr}$ = 0.10 ± 0.05‰, 2SD; Gleeson et al., 2020; Teng et al., 2013). It is noteworthy that the $\delta^{57}Fe_{corr}$ values of the classic HIMU OIBs ($\delta^{57}Fe_{corr}$ = 0.06–0.15‰) are consistent with those of peridotite-derived melts rather than eclogite-derived melts with higher $\delta^{57}Fe_{corr}$ values (Fig. 5A). This implies a peridotite-dominated mantle source for these OIBs.

The redox state of the mantle source may also influence the fractionation of Fe isotopes during melting (e.g., Dauphas et al., 2009, 2014). In Fig. 4C, the $Fe^{3+}/\Sigma Fe$ ratios of HIMU lavas are negatively correlated with their MgO contents, and the high MgO samples (MgO > 10 wt%) have $Fe^{3+}/\Sigma Fe$ ratios of ~0.2. Hence, we estimate that the $Fe^{3+}/\Sigma Fe$ of the primary HIMU magmas is about 0.2. This value is

slightly higher than that of MORBs ($Fe^{3+}/\Sigma Fe = 0.14 \pm 0.02$; Zhang et al., 2018), suggesting a more oxidized mantle source for HIMU lavas compared to MORBs. This is consistent with previous calculations based on the vanadium contents of olivine phenocrysts in HIMU lavas, which indicate that the HIMU mantle source has a higher oxygen fugacity than the depleted MORB mantle (Nicklas et al., 2022). Therefore, we calculated the Fe isotope fractionation ($\Delta^{57}Fe_{melt\text{-}source}$) during melting under different redox conditions ($Fe^{3+}/\Sigma Fe$ ratios in the mantle source vary between 0.03 and 0.07), following the approach of Dauphas et al. (2014). The calculated results show that the assumed changes in redox conditions have a limited effect on Fe isotopic fractionation (Fig. 5B). This observation is similar to that in Sossi and O'Neill (2017): even if the $Fe^{3+}/\Sigma Fe$ ratios in the mantle source changed from 0.021 (reduced) to 0.051 (oxidized), the difference in Fe isotopic fractionation is <0.02‰. In short, even when considering the effect of slightly higher oxygen fugacity in the HIMU mantle source, our observation that the HIMU mantle source is peridotite-dominated will not change.

5.3. Carbonated peridotite source for the classic HIMU OIBs

The MORB-like Fe isotope compositions of classic HIMU OIBs indicate that their mantle source is most likely to be peridotitic, consistent with previous observations from the low Ni contents (mostly <2000 ppm) and high Mn/Fe ratios (100Mn/Fe = 1.5–1.7) of olivine phenocrysts in Mangaia and Tubuai HIMU lavas (Herzberg et al., 2014; Weiss et al., 2016). Such Ni contents and Mn/Fe ratios are close to those of olivine phenocrysts in MORBs (Sobolev et al., 2007; **Fig. S2**). Meanwhile, in the CaO-MgO diagram advocated by Herzberg and Asimow (2008), the relatively primitive HIMU lavas (e.g., MgO > 9 wt%) are plotted in the field for peridotite-derived melts or their evolved melts that have only undergone olivine fractionation (**Fig. S3**).

However, previous geochemical observations have suggested that recycled ancient oceanic crust should be an 'ingredient' of the HIMU component. For example, the moderately high $^{187}Os/^{188}Os$ (0.14–0.15) ratios of HIMU lavas require mixing between subducted oceanic crust-derived melt and the ambient mantle peridotite (Hanyu et al., 2011a). The low $^{3}He/^{4}He$ ratios (e.g., 5–8 R_A; Hanyu and Kaneoka, 1997; Hanyu et al., 2011b, 2014) of HIMU OIBs also indicate contributions from recycled oceanic crust. Since recycled oceanic crust has higher (U + Th)/^{3}He ratios than the ambient mantle, it will be characterized by high ^{4}He contents and low $^{3}He/^{4}He$ ratios after long-term α decay of U and Th (e.g., Hanyu et al., 2011b, 2014; Hanyu and Kaneoka, 1997). Moreover, melt inclusions in olivine phenocrysts of HIMU lavas have higher Cl/K (~ 0.076, mean value) and Cl/Nb (~ 10.4, mean value) ratios (Hanyu et al., 2019) compared to N-MORBs with Cl/K of ~0.02 and Cl/Nb of ~5 (Shimizu et al., 2016), which also requires contribution from subducted altered oceanic crust. Additionally, there are also some stable isotopic fingerprints of recycled oceanic crust in the HIMU OIBs, such as the moderately elevated $\delta^{7}Li$ (up to 6.2‰; Chan et al., 2009), the mass-independent fractionation of sulfur isotopes (Cabral et al., 2013), and the generally lower $\varepsilon^{205}Tl$ values (down to −9.8; Blusztajn et al., 2018).

On the other hand, several lines of evidence support the idea that the HIMU mantle source may have undergone metasomatism by carbonatite/carbonated silicate melts or may contain some recycled carbonates: (1) the primitive HIMU OIBs are SiO_2-undersaturated and have high CaO contents and CaO/Al_2O_3 ratios (Figs. 3A-B) (Castillo, 2015; Dasgupta et al., 2010; Hanyu et al., 2011a; Jackson and Dasgupta, 2008; Kawabata et al., 2011); (2) the incompatible trace element patterns of HIMU OIBs are similar to those of carbonatitic melt inclusions in diamonds (Weiss et al., 2016); (3) olivine phenocrysts in HIMU OIBs show obviously higher Ca/Al ratios (mean value >20) compared to those in MORBs (mean value <10; Sobolev et al., 2007) (**Fig. S2**; Weiss et al., 2016); (4) the extremely heavy zinc isotopic compositions ($\delta^{66}Zn = 0.38 \pm 0.03$‰) of HIMU lavas indicate that recycled surficial carbonates have contributed to the HIMU mantle source (Zhang et al., 2022).

Previous studies have proposed different models to reconcile the peridotitic HIMU source with the observed geochemical imprints of ancient recycled oceanic crust and carbonate. For instance, Herzberg et al. (2014) proposed that recycled oceanic crust no longer exists in the HIMU source, while its released melts modified the geochemical compositions of the surrounding peridotite and yielded a refertilized peridotite. Weiss et al. (2016) further proposed that the HIMU source is carbonatite-metasomatized SCLM associated with ancient oceanic crust subduction. Zhang et al. (2022) suggested that carbonate-bearing melts formed through the partial melting of subducted oceanic crust (and overlying carbonates) metasomatized the surrounding mantle, ultimately creating the carbonated peridotite source for the HIMU OIBs. These models have one thing in common: the recycled oceanic crust and/or carbonate have contributed to the generation of the HIMU component through an indirect way. However, a new question arises regarding whether the observations on Fe isotopic compositions in this study can be reconciled with these scenarios.

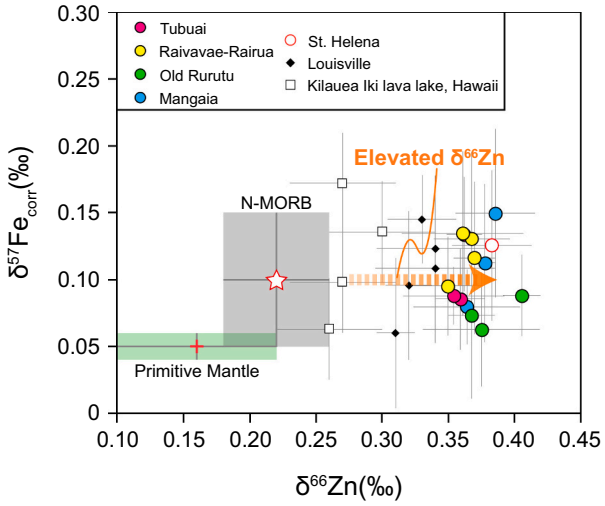

Fig. 6. $\delta^{57}Fe_{corr}$ versus $\delta^{66}Zn$ for Cook-Austral HIMU OIB samples. The Fe isotope data have been corrected for fractional crystallization (see Section 5.1 for detail). Also shown are literature data for basalts from St. Helena, Louisville, and Kilauea Iki lava lake (Hawaii). Data sources for Fe isotopes: St. Helena (Zhao et al., 2022), Louisville (Shi et al., 2022), Kilauea Iki lava lake (Hawaii; Teng et al., 2008), N-MORB ($\delta^{57}Fe_{corr} = 0.10 \pm 0.05$‰; Gleeson et al., 2020; Teng et al., 2013), primitive mantle ($\delta^{57}Fe = 0.05 \pm 0.01$‰; Sossi et al., 2016). Data sources for Zn isotopes: St. Helena and Louisville (Zhang et al., 2022), Kilauea Iki lava lake (Chen et al., 2013), N-MORBs ($\delta^{66}Zn = 0.22 \pm 0.04$‰; Sun et al., 2023), primitive mantle ($\delta^{66}Zn = 0.16 \pm 0.06$‰; Sossi et al., 2018). Error bars represent 2SD uncertainties.

Experimental work suggests that the descending carbonated oceanic crust can release carbonatitic/carbonated silicate melts at the depth of the mantle transition zone (MTZ) (e.g., Thomson et al., 2016; Zhang et al., 2020). The experimental carbonate-bearing melts in the pressure and temperature conditions of MTZ have FeO_T (6–8 wt%; Thomson et al., 2016; Zhang et al., 2020) contents similar to those of the primitive mantle (8.03 wt%; McDonough and Sun, 1995). Since Fe in subducted oceanic crust is mainly hosted in silicates, the carbonate-bearing melts produced by the melting of subducted carbonated oceanic crust are expected to show similar heavy Fe isotopic compositions (e.g., 0.21–0.23‰; Fig. 5A **and Table S4**) to those of modelled silicate melts derived from eclogite. Thus, the Fe isotopic compositions of metasomatized peridotite formed by the addition of such carbonate-bearing melts into normal peridotite will be slightly elevated (Fig. 6). For example, modelling calculation shows that the addition of ~30% carbonate-bearing melts (assumed $FeO_T = 7$ wt%, $\delta^{57}Fe = 0.23$‰) into a normal peridotite ($FeO_T = 8.03$ wt%, McDonough and Sun, 1995; $\delta^{57}Fe = 0.05$‰, Sossi et al., 2016) can form a carbonated peridotite with a $\delta^{57}Fe$ value of ~0.09‰. The partial melting of such a carbonated peridotite

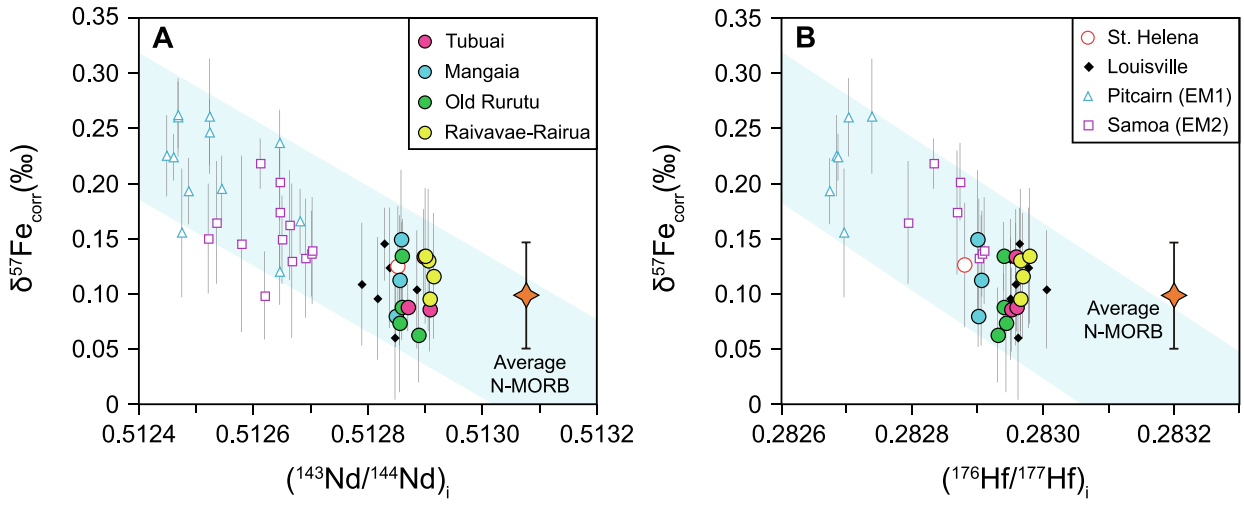

Fig. 7. $\delta^{57}Fe_{corr}$ versus (A) $(^{143}Nd/^{144}Nd)_i$ and (B) $(^{176}Hf/^{177}Hf)_i$ ratios for Cook-Austral HIMU OIB samples. Also shown are literature data for endmember OIBs from St. Helena, Louisville, Pitcairn, and Samoa. The Fe isotope data have been corrected for fractional crystallization (see Section 5.1 for detail). Data sources for Fe isotopes: St. Helena (Zhao et al., 2022), Louisville (Shi et al., 2022), Pitcairn (Nebel et al., 2019; Shi et al., 2022), Samoa (Soderman et al., 2021; Wang et al., 2021), average N-MORBs (Gleeson et al., 2020; Teng et al., 2013). Data sources for $(^{143}Nd/^{144}Nd)_i$ and $(^{176}Hf/^{177}Hf)_i$: Cook-Austral islands (Hanyu et al., 2011a; Miyazaki et al., 2018), St. Helena (Hanyu et al., 2014), Louisville (Shi et al., 2022), Pitcairn (Tedside) (Nebel et al., 2019 and references therein; Wang et al., 2018), Samoa (Malumalu trend) (Soderman et al., 2021 and references therein; Wang et al., 2021), average N-MORBs (Gale et al., 2013).

can explain the slightly higher $\delta^{57}Fe_{corr}$ (~ 0.14‰) values of some HIMU lavas (Fig. 5A). Meanwhile, the partial melting of subducted oceanic crust (along with overlying carbonate sediments) can release carbonate-bearing melts with higher $\delta^{66}Zn$ values and Zn contents than ambient peridotite (e.g., Wang et al., 2022; Zhang et al., 2022). Such carbonate-bearing melts will significantly alter the Zn isotopic compositions of the ambient peridotite and produce a carbonated peridotite with a high $\delta^{66}Zn$ signature (e.g., 0.3‰; Zhang et al., 2022). In addition, since the carbonate-bearing melts released by subducted oceanic crust have MgO contents (generally <7.0 wt%; Thomson et al., 2016) far lower than mantle peridotite, their addition to peridotite has minimal impact on the Mg isotopic compositions of the latter (Chen et al., 2022). This explains the observation of MORB-like $\delta^{26}Mg$ values (e.g., − 0.25‰; Wang et al., 2021) in primary St. Helena HIMU lavas. In summary, the partial melting of a carbonated peridotite, formed by the interaction between carbonate-bearing melts from subducting carbonated oceanic crust (plus carbonate sediments) and the surrounding peridotite, can well explain the MORB-like Fe and Mg isotopic compositions and the distinctly heavy Zn isotopic signature of HIMU OIBs (Fig. 6).

5.4. Summary and implication

The MORB-like Fe isotopic compositions, combined with heavy whole-rock zinc isotopic compositions ($\delta^{66}Zn = 0.37 \pm 0.03$‰; Zhang et al., 2022) and characteristic olivine phenocryst compositions (high Mn/Fe and Ca/Al ratios; Herzberg et al., 2014; Weiss et al., 2016) in these HIMU lavas, provide further evidence that the HIMU mantle source may consist of carbonated peridotite. In comparison, previous Fe isotopic studies on EM1-type OIBs from Pitcairn Island and EM2-type OIBs from Samoa islands/seamounts suggest that their mantle sources contain significant amounts of pyroxenite/eclogite transformed from recycled crustal materials (Nebel et al., 2019; Shi et al., 2022; Soderman et al., 2021; Wang et al., 2021). As a whole, the $\delta^{57}Fe_{corr}$ values of all OIBs from the type localities for the several mantle components clearly show a negative correlation with radiogenic Nd and Hf isotopic compositions (Fig. 7). The combination of Fe stable isotopes and long-lived radiogenic isotopes in OIBs provides new insights into ancient crust-mantle processes and related mantle dynamics. Specifically, (1) the heterogeneity in radiogenic isotopic compositions of the mantle is closely linked to the lithological heterogeneity (e.g., Gleeson et al., 2020; Nebel et al., 2019; Shi et al., 2022; Wang et al., 2021); and (2) the variable Fe isotopic compositions of OIBs can reflect the different fates of recycled crustal materials in the mantle. Some recycled crustal materials have been directly incorporated into the mantle source of geochemically enriched basalts, such as EM1 and EM2 OIBs, while others have indirectly contributed to the generation of geochemically depleted basalts, such as HIMU OIBs and some MORBs, through processes like metasomatism.

Declaration of competing interest

The authors declare that they have no known competing financial interests or personal relationships that could have appeared to influence the work reported in this paper.

Acknowledgements

This study was financially supported by the National Natural Science Foundation of China (grants 42130310, 41973001). The insightful editorial handling of Prof. Di-Cheng Zhu and the constructive comments from two anonymous reviewers significantly improved the manuscript. We are grateful to Prof. Jin-Hui Yang, Prof. Yue-Heng Yang and Dr. Chao Huang for their laboratory or technical supports. Dr. Yuan Zhong and Jin-Hua Shi are thanked for their help with the Fe isotope analysis.

Appendix A. Supplementary data

Supplementary data to this article can be found online at https://doi.org/10.1016/j.lithos.2024.107531.

References

Blusztajn, J., Nielsen, S.G., Marschall, H.R., Shu, Y., Ostrander, C.M., Hanyu, T., 2018. Thallium isotope systematics in volcanic rocks from St. Helena – Constraints on the origin of the HIMU reservoir. Chem. Geol. 476, 292–301.

Brounce, M., Stolper, E., Eiler, J., 2022. The mantle source of basalts from Reunion Island is not more oxidized than the MORB source mantle. Contrib. Mineral. Petrol. 177, 7. https://doi.org/10.1007/s00410-021-01870-w.

Cabral, R.A., Jackson, M.G., Rose-Koga, E.F., Koga, K.T., Whitehouse, M.J., Antonelli, M. A., Farquhar, J., Day, J.M.D., Hauri, E.H., 2013. Anomalous Sulphur isotopes in plume lavas reveal deep mantle storage of Archaean crust. Nature 496, 490–493.

Castillo, P.R., 2015. The recycling of marine carbonates and sources of HIMU and FOZO Ocean island basalts. Lithos 216, 254–263.

Chan, L.H., Lassiter, J.C., Hauri, E.H., Hart, S.R., Blusztajn, J., 2009. Lithium isotope systematics of lavas from the Cook–Austral Islands: Constraints on the origin of HIMU mantle. Earth Planet. Sci. Lett. 277 (3–4), 433–442.
Chauvel, C., Hofmann, A.W., Vidal, P., 1992. HIMU-EM: the French Polynesian connection. Earth Planet. Sci. Lett. 110, 99–119.
Chen, H., Savage, P.S., Teng, F.-Z., Helz, R.T., Moynier, F., 2013. Zinc isotope fractionation during magmatic differentiation and the isotopic composition of the bulk Earth. Earth Planet. Sci. Lett. 369, 34–42.
Chen, L.-H., Wang, X.-J., Liu, S.-A., 2022. Probing recycled carbonate in the lower mantle. Natl. Sci. Rev. 9 https://doi.org/10.1093/nsr/nwac061.
Chen, S., Niu, Y., Guo, P., Gong, H., Sun, P., Xue, Q., Duan, M., Wang, X., 2019. Iron isotope fractionation during mid-ocean ridge basalt (MORB) evolution: evidence from lavas on the East Pacific rise at 10°30′N and its implications. Geochim. Cosmochim. Acta 267, 227–239.
Chen, Y.H., Niu, Y.L., Duan, M., Gong, H.M., Guo, P.Y., 2021. Fractional crystallization causes the iron isotope contrast between mid-ocean ridge basalts and abyssal peridotites. Commun. Earth & Environ. 2 (1) https://doi.org/10.1038/s43247-021-00135-5.
Craddock, P.R., Warren, J.M., Dauphas, N., 2013. Abyssal peridotites reveal the near-chondritic Fe isotopic composition of the Earth. Earth Planet. Sci. Lett. 365, 63–76.
Dasgupta, R., Jackson, M.G., Lee, C.-T.A., 2010. Major element chemistry of ocean island basalts — Conditions of mantle melting and heterogeneity of mantle source. Earth Planet. Sci. Lett. 289, 377–392.
Dauphas, N., Craddock, P.R., Asimow, P.D., Bennett, V.C., Nutman, A.P., Ohnenstetter, D., 2009. Iron isotopes may reveal the redox conditions of mantle melting from Archean to present. Earth Planet. Sci. Lett. 288, 255–267.
Dauphas, N., Janney, P.E., Mendybaev, R.A., Wadhwa, M., Richter, F.M., Davis, A.M., Van Zuilen, M., Hines, R., Foley, C.N., 2004. Chromatographic separation and multicollection-ICPMS analysis of iron. Investigating mass-dependent and-independent isotope effects. Anal. Chem. 76, 5855–5863.
Dauphas, N., Roskosz, M., Alp, E.E., Neuville, D.R., Hu, M.Y., Sio, C.K., Tissot, F.L.H., Zhao, J., Tissandier, L., Médard, E., Cordier, C., 2014. Magma redox and structural controls on iron isotope variations in Earth's mantle and crust. Earth Planet. Sci. Lett. 398, 127–140.
French, S.W., Romanowicz, B., 2015. Broad plumes rooted at the base of the Earth's mantle beneath major hotspots. Nature 525, 95–99.
Gale, A., Dalton, C.A., Langmuir, C.H., Su, Y., Schilling, J., 2013. The mean composition of ocean ridge basalts. Geochem. Geophys. Geosyst. 14 (3), 489–518. https://doi.org/10.1029/2012GC004334.
Gleeson, M.L.M., Gibson, S.A., Williams, H.M., 2020. Novel insights from Fe-isotopes into the lithological heterogeneity of Ocean Island Basalts and plume-influenced MORBs. Earth Planet. Sci. Lett. 535, 116114 https://doi.org/10.1016/j.epsl.2020.116114.
Graham, D.W., 2002. Noble Gas Isotope Geochemistry of Mid-Ocean Ridge and Ocean Island Basalts: Characterization of Mantle Source Reservoirs. Rev. Mineral. Geochem. 47 (1), 247–317.
Hanyu, T., Chen, L.-H., 2021. Geochemical Diversity in the Mantle, Mantle Convection and Surface Expressions, pp. 121–150. https://doi.org/10.1002/9781119528609.ch5.
Hanyu, T., Kaneoka, I., 1997. The uniform and low $^{3}He/^{4}He$ ratios of HIMU basalts as evidence for their origin as recycled materials. Nature 390, 273–276.
Hanyu, T., Kawabata, H., Tatsumi, Y., Kimura, J.-I., Hyodo, H., Sato, K., Miyazaki, T., Chang, Q., Hirahara, Y., Takahashi, T., Senda, R., Nakai, S.I., 2014. Isotope evolution in the HIMU reservoir beneath St. Helena: Implications for the mantle recycling of U and Th. Geochim. Cosmochim. Acta 143, 232–252.
Hanyu, T., Shimizu, K., Ushikubo, T., Kimura, J.-I., Chang, Q., Hamada, M., Ito, M., Iwamori, H., Ishikawa, T., 2019. Tiny droplets of ocean island basalts unveil Earth's deep chlorine cycle. Nat. Commun. 10, 60. https://doi.org/10.1038/s41467-018-07955-8.
Hanyu, T., Tatsumi, Y., Kimura, J., 2011b. Constraints on the origin of the HIMU reservoir from He–Ne–Ar isotope systematics. Earth Planet. Sci. Lett. 307 (3–4), 377–386.
Hanyu, T., Tatsumi, Y., Senda, R., Miyazaki, T., Chang, Q., Hirahara, Y., Takahashi, T., Kawabata, H., Suzuki, K., Kimura, J.-I., Nakai, S.I., 2011a. Geochemical characteristics and origin of the HIMU reservoir: a possible mantle plume source in the lower mantle. Geochem. Geophys. Geosyst. 12 https://doi.org/10.1029/2010GC003252.
Hart, S.R., 1984. A large-scale isotope anomaly in the Southern Hemisphere mantle. Nature 309, 753–757.
Hart, S.R., Hauri, E.H., Oschmann, L.A., Whitehead, J.A., 1992. Mantle Plumes and Entrainment: Isotopic evidence. Science 256, 517–520.
Herzberg, C., Asimow, P.D., 2008. Petrology of some oceanic island basalts: PRIMELT2.XLS software for primary magma calculation. Geochem. Geophys. Geosyst. 9 https://doi.org/10.1029/2008GC002057.
Herzberg, C., Cabral, R.A., Jackson, M.G., Vidito, C., Day, J.M.D., Hauri, E.H., 2014. Phantom Archean crust in Mangaia hotspot lavas and the meaning of heterogeneous mantle. Earth Planet. Sci. Lett. 396, 97–106.
Hofmann, A.W., 1997. Mantle geochemistry: the message from oceanic volcanism. Nature 385, 219–229.
Hofmann, A.W., White, W.M., 1982. Mantle plumes from ancient oceanic crust. Earth Planet. Sci. Lett. 57, 421–436.
Homrighausen, S., Hoernle, K., Hauff, F., Geldmacher, J., Wartho, J.-A., van den Bogaard, P., Garbe-Schönberg, D., 2018. Global distribution of the HIMU end member: Formation through Archean plume-lid tectonics. Earth Sci. Rev. 182, 85–101.
Imai, N., Terashima, S., Itoh, S., Ando, A., 1995. 1994 compilation values for GSJ reference samples, “Igneous rock series&rdquo. Geochem. J. 29, 91–95.
Jackson, M.G., Dasgupta, R., 2008. Compositions of HIMU, EM1, and EM2 from global trends between radiogenic isotopes and major elements in ocean island basalts. Earth Planet. Sci. Lett. 276 (1–2), 175–186.
Kawabata, H., Hanyu, T., Chang, Q., Kimura, J.-I., Nichols, A.R.L., Tatsumi, Y., 2011. The Petrology and Geochemistry of St. Helena Alkali Basalts: Evaluation of the Oceanic Crust-recycling Model for HIMU OIB. J. Petrol. 52, 791–838.
Kimura, J.I., Gill, J.B., Skora, S., van Keken, P.E., Kawabata, H., 2016. Origin of geochemical mantle components: Role of subduction filter. Geochem. Geophys. Geosyst. 17, 3289–3325.
Konter, J.G., Pietruszka, A.J., Hanan, B.B., Finlayson, V.A., Craddock, P.R., Jackson, M.G., Dauphas, N., 2016. Unusual $\delta^{56}Fe$ values in Samoan rejuvenated lavas generated in the mantle. Earth Planet. Sci. Lett. 450, 221–232.
Le Bas, M.J., Le Maitre, R.W., Streckeisen, A., Zanettin, B., 1986. A Chemical Classification of Volcanic Rocks based on the Total Alkali-Silica Diagram. J. Petrol. 27 (3), 745–750.
MacDonald, G.A., Katsura, T., 1964. Chemical composition of Hawaiian lavas. J. Petrol. 5, 82–133.
Maury, R.C., Guille, G., Guillou, H., Chauvel, C., Rossi, P., Pallares, C., Legendre, C., 2013. Temporal evolution of a Polynesian hotspot: New evidence from Raivavae (Austral islands, South Pacific Ocean). Bulletin de la Société géologique de France 184, 557–567.
McCoy-West, A.J., Fitton, J.G., Pons, M.-L., Inglis, E.C., Williams, H.M., 2018. The Fe and Zn isotope composition of deep mantle source regions: Insights from Baffin Island picrites. Geochim. Cosmochim. Acta 238, 542–562.
McDonough, W.F., Sun, S.-S., 1995. The composition of the Earth. Chem. Geol. 120, 223–253.
Miyazaki, T., Hanyu, T., Kimura, J.-I., Senda, R., Vaglarov, B.S., Chang, Q., Hirahara, Y., Takahashi, T., Kawabata, H., Sato, T., 2018. Clinopyroxene and bulk rock Sr–Nd–Hf–Pb isotope compositions of Raivavae Ocean island basalts: does clinopyroxene record early stage magma chamber processes? Chem. Geol. 482, 18–31.
Nebel, O., Sossi, P.A., Bénard, A., Arculus, R.J., Yaxley, G.M., Woodhead, J.D., Rhodri Davies, D., Ruttor, S., 2019. Reconciling petrological and isotopic mixing mechanisms in the Pitcairn mantle plume using stable Fe isotopes. Earth Planet. Sci. Lett. 521, 60–67.
Nicklas, R.W., Hahn, R.K.M., Willhite, L.N., Jackson, M.G., Zanon, V., Arevalo, R., Day, J.M.D., 2022. Oxidized mantle sources of HIMU- and EM-type Ocean Island Basalts. Chem. Geol. 602, 120901 https://doi.org/10.1016/j.chemgeo.2022.120901.
Pietruszka, A.J., Norman, M.D., Garcia, M.O., Marske, J.P., Burns, D.H., 2013. Chemical heterogeneity in the Hawaiian mantle plume from the alteration and dehydration of recycled oceanic crust. Earth Planet. Sci. Lett. 361, 298–309.
Polyakov, V.B., Mineev, S.D., 2000. The use of Mössbauer spectroscopy in stable isotope geochemistry. Geochim. Cosmochim. Acta 64, 849–865.
Rose, J., Koppers, A.A., 2019. Simplifying age progressions within the Cook-Austral islands using ARGUS-VI high-resolution $^{40}Ar/^{39}Ar$ incremental heating ages. Geochem. Geophys. Geosyst. 20, 4756–4778.
Ryan, W.B.F., Carbotte, S.M., Coplan, J.O., O'Hara, S., Melkonian, A., Arko, R., Weissel, R.A., Ferrini, V., Goodwillie, A., Nitsche, F., Bonczkowski, J., Zemsky, R., 2009. Global Multi-Resolution Topography synthesis. Geochem. Geophys. Geosyst. 10 https://doi.org/10.1029/2008GC002332.
Schuessler, J.A., Schoenberg, R., Sigmarsson, O., 2009. Iron and lithium isotope systematics of the Hekla volcano, Iceland — evidence for Fe isotope fractionation during magma differentiation. Chem. Geol. 258, 78–91.
Shi, J.H., Zeng, G., Chen, L.H., Hanyu, T., Wang, X.J., Zhong, Y., Xie, L.W., Xie, W.L., 2022. An eclogitic component in the Pitcairn mantle plume: evidence from olivine compositions and Fe isotopes of basalts. Geochim. Cosmochim. Acta 318, 415–427.
Shimizu, K., Saal, A.E., Myers, C.E., Nagle, A.N., Hauri, E.H., Forsyth, D.W., Kamenetsky, V.S., Niu, Y., 2016. Two-component mantle melting-mixing model for the generation of mid-ocean ridge basalts: Implications for the volatile content of the Pacific upper mantle. Geochim. Cosmochim. Acta 176, 44–80.
Sobolev, A.V., Hofmann, A.W., Kuzmin, D.V., Yaxley, G.M., Arndt, N.T., Chung, S.-L., Danyushevsky, L.V., Elliott, T., Frey, F.A., Garcia, M.O., Gurenko, A.A., Kamenetsky, V.S., Kerr, A.C., Krivolutskaya, N.A., Matvienkov, V.V., Nikogosian, I.K., Rocholl, A., Sigurdsson, I.A., Sushchevskaya, N.M., Teklay, M., 2007. The Amount of Recycled Crust in sources of Mantle-Derived Melts. Science 316, 412–417.
Soderman, C.R., Matthews, S., Shorttle, O., Jackson, M.G., Ruttor, S., Nebel, O., Turner, S., Beier, C., Millet, M.-A., Widom, E., Humayun, M., Williams, H.M., 2021. Heavy $\delta^{57}Fe$ in ocean island basalts: a non-unique signature of processes and source lithologies in the mantle. Geochim. Cosmochim. Acta 292, 309–332.
Soderman, C.R., Shorttle, O., Gazel, E., Geist, D.J., Matthews, S., Williams, H.M., 2023. The evolution of the Galapagos mantle plume. Science. Advances 9, eadd5030. https://doi.org/10.1126/sciadv.add5030.
Soderman, C.R., Shorttle, O., Matthews, S., Williams, H.M., 2022. Global trends in novel stable isotopes in basalts: Theory and observations. Geochim. Cosmochim. Acta 318, 388–414.
Sossi, P.A., Foden, J.D., Halverson, G.P., 2012. Redox-controlled iron isotope fractionation during magmatic differentiation: an example from the Red Hill intrusion, S. Tasmania. Contrib. Mineral. Petrol. 164, 757–772.
Sossi, P.A., Nebel, O., Foden, J., 2016. Iron isotope systematics in planetary reservoirs. Earth Planet. Sci. Lett. 452, 295–308.
Sossi, P.A., Nebel, O., O'Neill, H.S.C., Moynier, F., 2018. Zinc isotope composition of the Earth and its behaviour during planetary accretion. Chem. Geol. 477, 73–84.
Sossi, P.A., O'Neill, H.S.C., 2017. The effect of bonding environment on iron isotope fractionation between minerals at high temperature. Geochim. Cosmochim. Acta 196, 121–143.

Stracke, A., 2012. Earth's heterogeneous mantle: a product of convection-driven interaction between crust and mantle. Chem. Geol. 330-331, 274–299.
Stracke, A., Hofmann, A.W., Hart, S.R., 2005. FOZO, HIMU, and the rest of the mantle zoo. Geochem. Geophys. Geosyst. 6 https://doi.org/10.1029/2004GC000824.
Sun, P., Niu, Y., Duan, M., Chen, S., Guo, P., Gong, H., Xiao, Y., Wang, X., 2023. Zinc isotope fractionation during mid-ocean ridge basalt differentiation: evidence from lavas on the East Pacific rise at 10° 30′ N. Geochim. Cosmochim. Acta 346, 180–191.
Teng, F.Z., Dauphas, N., Helz, R.T., 2008. Iron isotope fractionation during magmatic differentiation in Kilauea Iki lava lake. Science 320, 1620–1622.
Teng, F.Z., Dauphas, N., Huang, S., Marty, B., 2013. Iron isotopic systematics of oceanic basalts. Geochim. Cosmochim. Acta 107, 12–26.
Thomson, A.R., Walter, M.J., Kohn, S.C., Brooker, R.A., 2016. Slab melting as a barrier to deep carbon subduction. Nature 529, 76–79.
Wang, X.J., Chen, L.H., Hanyu, T., Shi, J.H., Zhong, Y., Kawabata, H., Miyazaki, T., Hirahara, Y., Takahashi, T., Senda, R., Chang, Q., Vaglarov, B.S., Kimura, J.I., 2021. Linking Chemical Heterogeneity to Lithological Heterogeneity of the Samoan Mantle Plume with Fe-Sr-Nd-Pb Isotopes. Journal of Geophysical Research: Solid. Earth 126. https://doi.org/10.1029/2021JB022887 e2021JB022887.
Wang, X.J., Chen, L.H., Hanyu, T., Zhou, Z.B., Liu, J.Q., Zeng, G., Zou, Z.Q., Bai, J.H., 2024. Calcium isotopic variability in hotspot lavas controlled by partial melting and source lithological heterogeneity. Chem. Geol. 644, 121857 https://doi.org/10.1016/j.chemgeo.2023.121857.
Wang, X.J., Chen, L.H., Hofmann, A.W., Hanyu, T., Kawabata, H., Zhong, Y., Xie, L.W., Shi, J.H., Miyazaki, T., Hirahara, Y., Takahashi, T., Senda, R., Chang, Q., Vaglarov, B.S., Kimura, J.I., 2018. Recycled ancient ghost carbonate in the Pitcairn mantle plume. Proc. Natl. Acad. Sci. 115, 8682–8687.
Wang, Z., Liu, S., Rudnick, R.L., Teng, F., Wang, S., Haggerty, S.E., 2022. Zinc isotope evidence for carbonate alteration of oceanic crustal protoliths of cratonic eclogites. Earth Planet. Sci. Lett. 580, 117394 https://doi.org/10.1016/j.epsl.2022.117394.
Weiss, Y., Class, C., Goldstein, S.L., Hanyu, T., 2016. Key new pieces of the HIMU puzzle from olivines and diamond inclusions. Nature 537, 666–670.
Weyer, S., Ionov, D.A., 2007. Partial melting and melt percolation in the mantle: the message from Fe isotopes. Earth Planet. Sci. Lett. 259, 119–133.
White, W.M., 2015. Probing the Earth's Deep Interior through Geochemistry. Geochem. Perspec. 4, 95–96.
Williams, H.M., Bizimis, M., 2014. Iron isotope tracing of mantle heterogeneity within the source regions of oceanic basalts. Earth Planet. Sci. Lett. 404, 396–407.
Williams, H.M., Peslier, A.H., McCammon, C., Halliday, A.N., Levasseur, S., Teutsch, N., Burg, J.P., 2005. Systematic iron isotope variations in mantle rocks and minerals: the effects of partial melting and oxygen fugacity. Earth Planet. Sci. Lett. 235, 435–452.
Williams, H.M., Prytulak, J., Woodhead, J.D., Kelley, K.A., Brounce, M., Plank, T., 2018. Interplay of crystal fractionation, sulfide saturation and oxygen fugacity on the iron isotope composition of arc lavas: an example from the Marianas. Geochim. Cosmochim. Acta 226, 224–243.
Zhang, H.L., Cottrell, E., Solheid, P.A., Kelley, K.A., Hirschmann, M.M., 2018. Determination of $Fe^{3+}/\Sigma Fe$ of XANES basaltic glass standards by Mössbauer spectroscopy and its application to the oxidation state of iron in MORB. Chem. Geol. 479, 166–175.
Zhang, X.Y., Chen, L.H., Wang, X.J., Hanyu, T., Hofmann, A.W., Komiya, T., Nakamura, K., Kato, Y., Zeng, G., Gou, W.X., Li, W.Q., 2022. Zinc isotopic evidence for recycled carbonate in the deep mantle. Nat. Commun. 13, 6085. https://doi.org/10.1038/s41467-022-33789-6.
Zhang, Y., Wang, C., Jin, Z., 2020. Decarbonation of stagnant slab in the mantle transition zone. Journal of Geophysical Research: Solid. Earth 125. https://doi.org/10.1029/2020JB019533 e2020JB019533.
Zhao, J., Wang, X.-J., Chen, L.-H., Hanyu, T., Shi, J.-H., Liu, X.-W., Kawabata, H., Xie, L.-W., 2022. The effect of Fe–Ti oxide separation on iron isotopic fractionation during basalt differentiation. Contrib. Mineral. Petrol. 177, 101. https://doi.org/10.1007/s00410-022-01967-w.
Zhong, Y., Chen, L.-H., Wang, X.-J., Zhang, G.-L., Xie, L.-W., Zeng, G., 2017. Magnesium isotopic variation of oceanic island basalts generated by partial melting and crustal recycling. Earth Planet. Sci. Lett. 463, 127–135.
Zindler, A., Hart, S., 1986. Chemical Geodynamics. Annu. Rev. Earth Planet. Sci. 14, 493–571.